Journal of Theoretical Medicine, Vol. 3, pp. 191-211
Reprints available directly from the publisher
Photocopying permitted by license only

A Model of Dispersion in Perifusion Systems

PAUL R. SHORTEN* and DAVID J.N. WALL†

Biomathematics Research Centre, Department of Mathematics & Statistics, University of Canterbury, Private Bag 4800, Christchurch, 1, New Zealand

(Received 4 September 2000)

The perifusion apparatus is an experimental tool used to model information transfer in endocrine systems. The major drawback of the perifusion system derives from the dispersion, diffusion and mixing of the hormone within the apparatus which distort the original released hormone concentration profile. In this paper we develop a mathematical model of the perifusion system that accounts for a number of observable features in the measured secretory profile. We also consider associated inverse problems, the solution of which enhance perifusion data measurements and unmask the underlying secretory events. In contrast with the raw data, the deconvolved data supports the concentration dependent, rapid activation of CRH-induced ACTH secretion. The perifusion chamber can be modeled by an advection-diffusion equation, and we develop general theory analysing the validity of this approximation. We also provide a characterisation of the degree of ill-posedness of the inverse advection-diffusion equation in terms of the perifusion parameters.

Keywords: Deconvolution; hormones; diffusion; advection; CRH; ACTH

1. INTRODUCTION

Information transfer in a number of endocrine systems occurs through rapid modulation of hormone levels in concentration pulses. The temporal architecture of the endocrine glandular signaling process is believed to convey important biochemical information to the target tissue, and also represents a signature of the responsive endocrine cells (Veldhuis, 1991). Therefore to understand the endocrine glandular physiology, the time domain structure of hormone synthesis and release is required. Such a quantitative understanding of the underlying glandular physiology is also a prerequisite for the formulation and testing of hypotheses of the underlying molecular mechanisms (LeBeau et al., 1997; Li et al., 1997; Shorten et al., 2000). This knowledge also aids in the understanding of various endocrine glandular pathophysiological conditions.

The perifusion apparatus is an *in vitro* experimental tool used to model the dynamics of information transfer in a number of endocrine systems (McIntosh and McIntosh, 1983; McIntosh et al., 1984; Evans et al., 1985). This transfer is mediated by the modulation of hormone concentration levels. The perifusion apparatus allows the hormonally stimulated release of hormones to be investigated. In this system, a liquid saline medium flowing at a constant rate, is pumped through the pipe over cells, which secrete a hormone

* Email address of P.R. Shorten: P.Shorten@math.canterbury.ac.nz
† Corresponding author: D.J.N. Wall Email address of D.J.N. Wall: D.Wall@math.canterbury.ac.nz

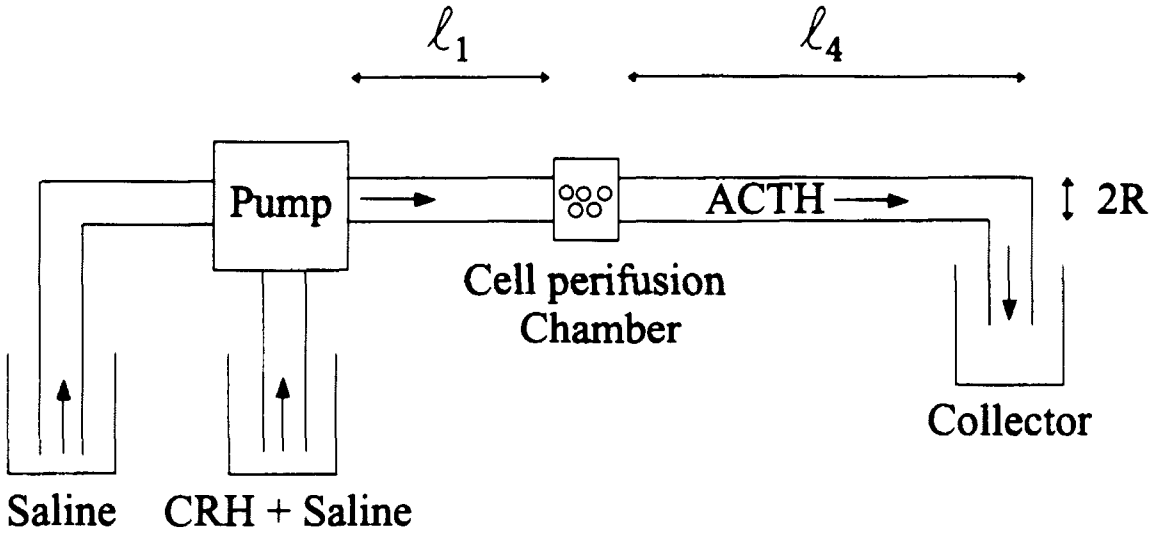

FIGURE 1 Schematic diagram of the perifusion apparatus. A saline solution carrying corticotropin releasing hormone (CRH) is pumped via a peristaltic pump down a pipe of length ℓ_1 to the cell perifusion chamber. A solenoid system allows the flowing medium to be switched between the saline and the CRH solutions. Corticotroph cells in the perifusion chamber then secrete adrenocorticotropic hormone (ACTH), which travels down a pipe of length ℓ_4 to the collector. The radius of the perifusion pipes is denoted by R

in response to another hormone in the flowing medium. The temporal concentration profile of this released substance is then measured at some downstream location. This downstream temporal measurement is a hormone concentration measurement averaged over the cross-section of the pipe. The pipe is typically 1 mm in diameter, and has a total length $(\ell_1 + \ell_4)$ of about 0.75 m. A schematic diagram of the perifusion apparatus is shown in Figure 1.

The perifusion chamber is a circular cylinder that is 4 mm in diameter and 25 mm in length, and typically contains about five million cells, predominantly in the top layer of a porous packing material (see Figure 2). This packing material is typically a combination of substances in the form of beads. The chamber is sealed with rubber plugs, pierced with a length of syringe needle over which is stretched a length of nylon cloth (10 μm pore size) to retain the contents of the column. The chamber is sealed within a thermojacket, allowing a constant cellular temperature of 37°C.

One may ask: What features does the engineering of the perifusion apparatus confer on the measured secretory profile?

The major drawback of the perifusion system derives from the dispersion, diffusion and mixing of the hormone in the tubing of the perifusion apparatus. This generates a distortion in the experimentally observed hormone concentration profile. In this paper we develop a mathematical model of the perifusion apparatus to understand this observed distortion in the hormone concentration profile. This model of the two dimensional fluid flow in the perifusion system accounts for a number of observable features in the measured secretory profile. Although this direct problem of prediction of elution concentration has been considered in connection with the perifusion apparatus (Smith et al., 1991), very little research has addressed associated inverse problems and their relevance to the improvement of data interpretation. In this paper we investigate these inverse problems, which are associated with the interesting mathematical problem of signal reconstruction after transmission through an advective and diffusive medium. We use the developed deconvolution strategies to enhance data measurements in the perifusion system, allowing the unmasking of the underlying secretory

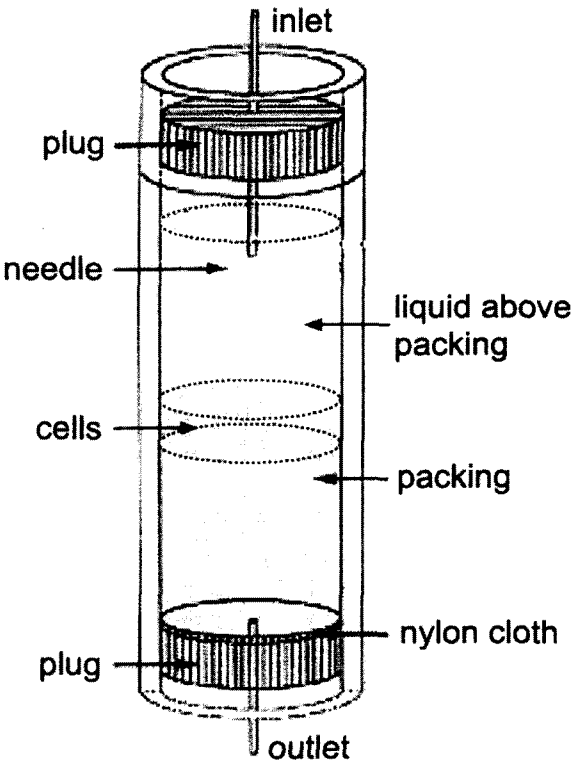

FIGURE 2 Schematic diagram of the perifusion chamber. Fluid flow into and out of the perifusion chamber is through needles of small diameter. Pituitary corticotroph cells lie in the top layer of the bead slurry packing. The bead packing material is a combination of Sephadex G25 and Bio-Gel P2, which absorb water and small molecules by diffusion, but not larger molecules such as ACTH. Based on figure from Smith et al. (1991)

events. However, due to the ill-posedness of the inverse problem, one cannot expect to completely remove the distortion in the measurement.

We have previously considered related inverse problems associated with the pure shear dispersive mass transport of a material concentration down a tube, when the flowing medium has a two-dimensional velocity profile (Shorten and Wall, 1998; Shorten and Wall, 2000). Although diffusive effects in the direction of fluid flow in the perifusion system are negligible, the contribution of molecular diffusion transverse to the direction of fluid flow is an important contributing factor in the observed distortion in perifusion experiments. The inverse problems considered in this paper also include this hormone diffusion. A number of researchers have incorporated this molecular diffusion into models of the perifusion chamber via an advection-diffusion equation (Kao, 1989; Smith et al., 1991). In this paper we also consider a general theory indicating under what conditions this approximation is valid, and how the parameters in the advection-diffusion model relate to measurable quantities in the perifusion system.

Hormone concentration levels are sometimes measured *in vivo*. In experiments associated with stress-levels in horses, a cannula tube is inserted *in vivo* to sample blood downstream from the pituitary, allowing cells to be monitored in their natural environment (Alexander et al., 1988). However blood displays a marked shear-dependent viscosity, and a finite yield stress may be necessary before flow can commence. Thus for the pipe diameters used in these experiments blood does not behave in a Newtonian manner. Although Newtonian fluids are specifically considered in this paper, the methods described here are also applicable in deconvolution problems associated with the non-Newtonian fluid flow in the aforementioned experiments (Shorten, 2000).

The paper plan is as follows. In Section 2 we develop a mathematical model of the perifusion system which is based on the experimental system of Evans et al. (1985). This model includes the shear dispersion, mixing, and molecular diffusion of the material tracer within the apparatus. In Section 3 we compare numerical solutions of the perifusion model with arginine vasopressin (AVP) pulse validation experiments. In Section 4 we consider the mathematics associated with the model. Section 4.1 outlines the Taylor approximation to the concentration dispersion within the pipe; a one-dimensional advection-diffusion equation. Section 4.2 discusses the importance of the model boundary conditions and their effect on the model solutions. In Section 5 we investigate the inverse problem of source reconstruction associated with the advection-diffusion equation. We consider the degree of ill-posedness of the inverse problem in Section 5.1, the problem regularisation in Section 5.2, and the construction of numerical schemes for the stabilised problem in Section 5.3. In Section 6 we illustrate our reconstruction algorithm for the perifusion

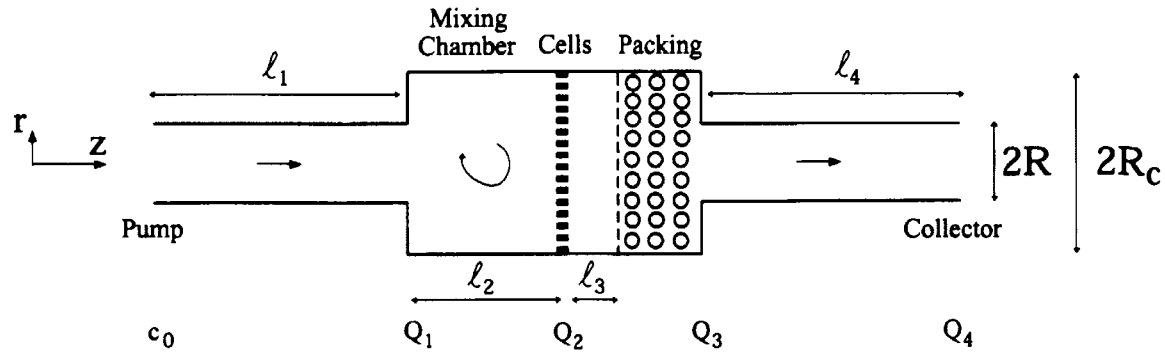

FIGURE 3 Schematic diagram of the perifusion apparatus illustrating the model geometry and location of the concentration symbols c_0, Q_1, Q_2, Q_3, and Q_4. The concentration symbol subscripts designate the geometric location of the different model stations

apparatus. In Section 7 we use the methods developed in the earlier sections to account for signal dispersion in CRH-induced ACTH measurements from equine corticotrophs.

2. THE PERIFUSION MODEL

The model of the perifusion apparatus includes the geometry of the system along with the shear dispersion, mixing, and molecular diffusion of the material tracer. A schematic diagram of the perifusion model geometry is shown in Figure 3.

The pipe from the pump to the perifusion chamber is 10^{-3} m in diameter ($2R$), and on average is 0.35 m in length (ℓ_1). The pipe from the chamber to the collector is also 10^{-3} m in diameter, and on average is 0.4 m in length (ℓ_4). The perifusion chamber is 2.5×10^{-2} m in length and 4×10^{-3} m in diameter ($2R_c$). Therefore the perifusion chamber volume is 0.31 mℓ. However, 20% of the chamber volume is filled by the plugs, (see Figure 2), and so the fluid before the cells comprises about 0.125 mℓ of the chamber volume. Thus the length of fluid from the chamber entrance to the pituitary cells is 0.01 m (ℓ_2). The cells are located in the centre of the chamber above the packing material (see Figure 2). The packing material fills about 60 % of the volume in the region between the pituitary cells and the chamber outlet. The packing material is largely settled in the lower part of the chamber. Therefore the volume of fluid in the chamber between the pituitary cells and the chamber outlet is 0.05 mℓ, and thus the length of fluid below the pituitary cells is 3.75×10^{-3} m (ℓ_3).

There are four different regions of fluid flow in the model of the perifusion system. The fluid is assumed to be Newtonian, and thus the fluid velocity profile of the viscous, incompressible fluid in the pipes is described by the well known Poiseuille distribution

$$v(r) = v_m \left(1 - \left(\frac{r}{R}\right)^2\right), \qquad (2.1)$$

where r is the circular polar radial coordinate associated with the cylindrical coordinate system so that the z-axis is aligned with the axis of the tube. The radius of the pipe is R, and the maximum flow velocity is v_m. The material tracer within the pipes undergoes shear dispersion, and diffusion across and along the pipe. For the Reynolds number associated with the perifusion system, the fluid flow in the pipes is fully developed after 6 pipe diameters (Knudsen and Katz, 1958), (p 228 *et seq.*). Therefore the region of developing flow is negligible in the pipes. However the flow within the chamber is slightly different. The fluid before the cells undergoes mixing (Mason, 2000), and we shall assume that the material tracer within this region is perfectly mixed. As the secreted ACTH does not enter the region before the cells and the length of pipe in the chamber between the pitui-

tary cells and the chamber outlet is small, the flow is assumed to be laminar and not developed within this region. Because the flow is not developed in the chamber between the pituitary cells and the chamber outlet, only axial diffusion need be considered. The packing material distribution effects the amount of diffusion that can occur. If the packing is evenly distributed and the flow rate is constant, then the amount of signal distortion is less than if the packing has settled to the lower part of the chamber. This is because the fluid travels faster through an evenly distributed packing material with no change in the diffusion coefficient. The flow rate through the perifusion system is 0.16 mℓ/min, and the travel time from the pump to the collector is about 150 s (Evans et al., 1988). It follows that υ_m, the maximum flow rate in the pipes, is 6.8×10^{-3} ms^{-1}, and $\overline{v_c}$, the average chamber fluid velocity, is 2.125×10^{-4} ms^{-1}. Note that the fluid velocity through the packing material is much greater than $\overline{v_c}$.

CRH, AVP, and ACTH have molecular weights of 1084, 4872, and 5500 Da respectively (Watanabe and Orth, 1987). These molecular weights allow the diffusion coefficients for these hormones in saline solution to be estimated (Weast, 1999; Washburn, 1926), and are shown in Table I along with the model parameters.

We now discuss the model equations. The cross-sectional average material concentration at the pump, chamber entrance, pituitary cells, chamber exit, and collector are denoted by c_0, Q_1, Q_2, Q_3, and Q_4 respectively (see Figure 3). The mass transport of the material tracer volume concentration, $c_1(z, r, t)$, in the pipe from the pump to the perifusion chamber can be modeled by

$$\frac{\partial c_1}{\partial t} + v(r)\frac{\partial c_1}{\partial z} = D\nabla^2 c_1, \quad z \in [0, \ell_1], \quad r \in [0,R], \quad t > 0, \tag{2.2}$$

where D is the coefficient of molecular diffusion, $\upsilon(r)$ is the Poiseuille distribution (2.1), and $\nabla^2 = \partial_z^2 + \partial_r^2 + \frac{1}{r}\partial_r$ is the Laplacian operator in circularly symmetric cylindrical coordinates. Because the injection of material into the pipe is independent of r, $c_1(0,r,t) = c_0(t)$. The net rate of change in the chamber concentration is the net amount of material entering the chamber per second divided by the chamber volume. That is

$$\frac{dQ_2}{dt} = \frac{2}{{R_c}^2 \ell_2}\int_0^R v(r)(c_1(\ell_1, r, t) - Q_2(t))rdr. \tag{2.3}$$

Integrating this equation we obtain the chamber output concentration

$$Q_2(t) = \frac{2}{{R_c}^2 \ell_2}\int_0^t \exp((s-t)/a_2)\int_0^R v(r)c_1(\ell_1, r, s)rdrds, \tag{2.4}$$

where

$$\frac{1}{a_2} = \frac{2}{{R_c}^2 \ell_2}\int_0^R v(r)rdr = \frac{\overline{v_c}}{\ell_2} \tag{2.5}$$

is the time of travel for fluid at the chamber centre to move a distance ℓ_2. The mass transport of the material tracer volume concentration, $c_3(z,t)$, in the chamber from the pituitary cells to the chamber outlet is given by

$$\frac{\partial c_3}{\partial t} + \overline{v_c}\frac{\partial c_3}{\partial z} = D\frac{\partial^2 c_3}{\partial z^2}, \quad z \in [0, \ell_3], \quad t > 0, \tag{2.6}$$

where z is now measured from the pituitary cells position and $c_3(0,t) = Q_2(t)$. The mass transport of the material tracer volume concentration, $c_4(z,r,t)$, in the pipe from the chamber to the collector is given by

$$\frac{\partial c_4}{\partial t} + v(r)\frac{\partial c_4}{\partial z} = D\nabla^2 c_4, \quad z \in [0, \ell_4], \quad r \in [0,R], \quad t > 0, \tag{2.7}$$

where z is now measured from the chamber exit. Because the injection of material into the pipe is again independent of r, $c_4(0,r,t) = c_3(\ell_3,t)$. At time $t = 0$ the initial concentration of the material tracer within the pipe is assumed to be zero, i.e.,

$$c_1(z,r,0) = Q_2(0) = c_3(z,0) = c_4(z,r,0) = 0,$$

and the walls of the pipes are assumed to be impermeable, so that

$$\left.\frac{\partial c_1}{\partial r}\right|_{r=R} = \left.\frac{\partial c_4}{\partial r}\right|_{r=R} = 0. \tag{2.8}$$

TABLE I Table of relevant model perifusion parameters

Parameter	*Definition*	*Value*
R	pipe radius	5×10^{-4} m
R_c	chamber radius	2×10^{-3} m
ℓ_1	input pipe length	0.35 m
ℓ_2	chamber mixing region length	0.01 m
ℓ_3	length of fluid below cells	3.75×10^{-3} m
ℓ_4	output pipe length	0.4 m
υ_m	maximum pipe fluid velocity	6.8×10^{-3} ms^{-1}
$\bar{v}$	average pipe fluid velocity	3.4×10^{-3} ms^{-1}
$\overline{v_c}$	average chamber fluid velocity	2.125×10^{-4} ms^{-1}
D_{CRH}	CRH diffusion coefficient	1.7×10^{-10} m^2·s^{-1}
D_{AVP}	AVP diffusion coefficient	3.5×10^{-10} m^2·s^{-1}
D_{ACTH}	ACTH diffusion coefficient	1.5×10^{-10} m^2·s^{-1}
η_{CRH}	effective CRH diffusion coefficient	3.5×10^{-4} m^2·s^{-1}
η_{AVP}	effective AVP diffusion coefficient	1.7×10^{-4} m^2·s^{-1}
η_{ACTH}	effective ACTH diffusion coefficient	4.0×10^{-4} m^2·s^{-1}

Because fluid flow into and out of the perifusion chamber is through needles of small diameter (see Figure 2), we assume that there is purely advective flow at these points, that is the diffusive flux is zero so that $\dfrac{\partial c_1}{\partial z}(\ell_1, t) = \dfrac{\partial c_3}{\partial z}(\ell_3, t) = 0$. Similarly at the collector there is purely advective flow with

$$\frac{\partial c_4}{\partial z}(\ell_4, t) = 0. \tag{2.9}$$

This boundary condition is termed Danckwerts' boundary condition (Smith, 1988), and therefore the material tracer cannot travel by diffusive means from the chamber to the inlet pipe, from the outlet pipe into the chamber, or from the collector into the outlet pipe; see Figures 1 and 3. Danckwerts' boundary condition is discussed further in Section 4.2. For simplicity, we shall also assume that there is no diffusive transport between the mixing chamber and the region between the pituitary cells and the chamber outlet. Given that the region before the pituitary cells is assumed to be perfectly mixed, this assumption does not significantly affect the problem solution.

3. PERIFUSION PULSE EXPERIMENTS

In this section we compare numerical solutions of the perifusion model developed in Section 2 with perifusion pulse validation experiments. In these experiments radioactively labelled arginine vasopressin (AVP) replaces the CRH shown in Figure 1. The radioactive AVP pulses are injected into the apparatus, and AVP concentrations are measured at the collector.

The model equations (2.2), (2.4), (2.6), and (2.7) relate the injected concentration profile to the concentration measured at the collector. Analytical solutions to (2.6) are available* (see Section 4.1), and (2.4) simply relates the chamber input concentration to the chamber concentration. However, simple analytical solutions to the direct problems (2.2) and (2.7) (along with boundary and initial conditions) are not readily available, and thus a numerical procedure must be employed to solve the direct problem. This problem is very well known, and there exists a multitude of approaches. The solution scheme considered here is an explicit finite difference scheme, where the opera-

* Note that (2.6) is a one-dimensional advection-diffusion equation whereas equations (2.2) and (2.7) are two-dimensional advection-diffusion equations

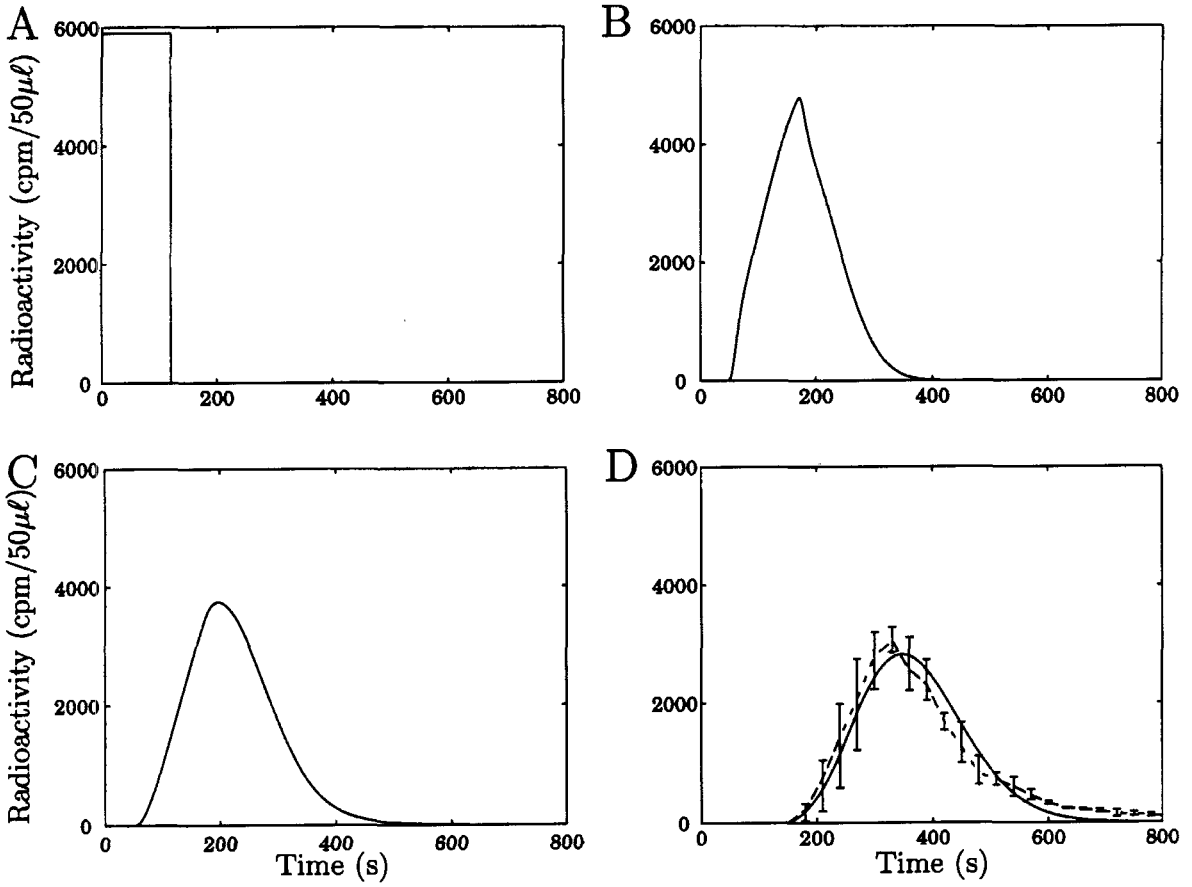

FIGURE 4 Comparison of the perifusion model and the 2 min pulse experimental data (Evans, 2000). (A) The input pulse c_0. (B) The model concentration at the chamber entrance Q_1. (C) The model concentration at the cells Q_2. (D) The model concentration at the collector, Q_4 (–), and the average of three experimental data sets (- – -). The error bars indicate the maximum and minimum values in the data sets, and cpm denotes counts per minute

tors ∂_t, ∂_z, ∂_z^2, ∂_r^2, and ∂_r in (2.2) and (2.7) are approximated by the finite difference operators δ_{t+}, δ_{z-}, δ_z^2, δ_r^2, and δ_{r0} respectively, where δ_-, δ_+, δ_0, and δ^2 are the backward, forward, central, and second central finite difference operators, respectively (Strikwerda, 1989). This is an explicit time stepping method, and if the time step is sufficiently small then the scheme is stable. This scheme provides sufficient resolution if the time step is appropriately small, and the spatial mesh sizes are smaller than their associated mesh Reynolds numbers (Strikwerda, 1989), (Section 6.4). Similar numerical results can also be obtained with the alternating direction implicit (A.D.I.) and locally one-dimensional (L.O.D.) methods, which are unconditionally stable.

Numerical simulations along with experimental results are shown in Figure 4. The numerical technique outlined above is used to predict the downstream cross-sectional average concentration profile generated by a 2 min upstream injection pulse of AVP with concentration 5900 cpm/50μℓ. The input pulse, c_0, is shown in Figure 4 A, Q_1 is shown in Figure 4 B, Q_2 is shown in Figure 4 C, and Q_4 is shown in Figure 4 D along with the experimental measurement

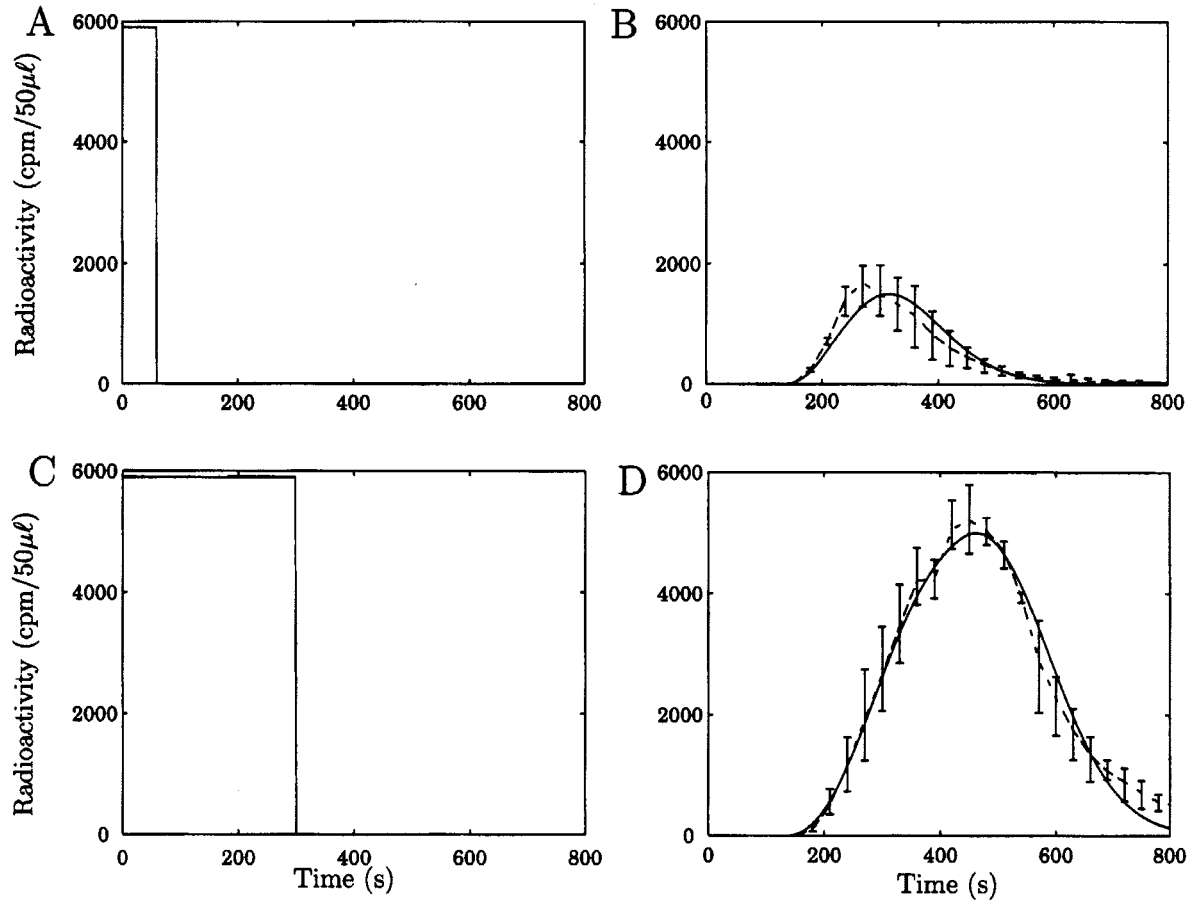

FIGURE 5 Comparison of the perifusion model (–) for the 1 and 5 min pulse experimental data (- – -). (A) The 1 min AVP injection pulse. (C) The 5 min AVP injection pulse. (B) The 1 min pulse is significantly attenuated, whereas (D) the 5 min pulse retains much of its original shape

(Evans, 2000). A linear spline (- – -) has been fitted through the average of three experimental data sets, and the error bars indicate the maximum and minimum values in the data sets. The pipes allow a moderate amount of dispersion of the pulse, and the mixing operator in (2.4) slightly delays the peak in concentration and smoothes the incoming pulse. Because the diffusion coefficient in (2.6) is a molecular diffusion coefficient, there is little dispersion in the perifusion chamber region from the cells to the chamber outlet, and therefore the functional form of Q_3 is very similar to Q_2 and is not shown.

The model prediction for 1, and 5 min upstream injection pulses is shown in Figure 5 B and D. There is significant attenuation of the 1 min pulse, whereas the 5 min pulse retains much of its original amplitude. These results show that the model, based on the fluid flow and the geometry of the system, agrees favourably with the experimental data, particularly for the longer pulses, where the relative amount of noise is lower.

The major discrepancy with the experimental data is that the predicted model concentration profiles decrease to zero at a faster rate. It is possible that the bead matrix in the chamber slightly impedes the flow

of the material tracer, thus delaying the decrease in the measured concentration profile. However it would be speculative to include such an effect in the model. The model also predicts slightly lower peak concentration levels. Possible causes of this are that the fluid is partially pseudoplastic, there is only partial mixing within the cell chamber, or we have slightly underestimated D_{AVP} for the saline solution. These three aspects all enable less dispersion. However, the current system data is not sufficiently accurate to elucidate the finer details of the dispersion.

4. DIFFUSIVE AND SHEAR DISPERSIVE FLOW

The basic phenomenon of dispersion in shear flow has been understood since Taylor, (1953) considered the direct problem of the transport of a diffusing material tracer injected into a Poiseuille flow. Many researchers have analysed the direct problem in more detail for a range of applications (Aris, 1953; Watt and Roberts, 1995; Phillips and Kaye, 1996). An inverse problem associated with the estimation of the molecular diffusion coefficient, from measured concentration profiles after dispersion, was also considered by Taylor, (1954). This inverse problem is one of the earliest inverse problem investigations in this area. We now consider a related inverse problem associated with dispersive flow in pipes. The inverse problem is that of finding $c_0(t)$ given measurements of the cross-sectional average concentration $Q_1(t)$. Simple analytical solutions to the direct problem (equation 2.2, along with boundary and initial conditions) are not readily available, and the inverse problem is therefore difficult to tackle. We proceed by constructing approximate solutions to the direct problem in this section, and the resulting inverse problems are considered in Section 5.

4.1. The Taylor approximation

Taylor, (1953) observed that under certain conditions, the dispersion of concentration in a pipe could be approximated by a more simple model, a one-dimensional advection-diffusion equation. That is, because of diffusive migration between different streamlines, the material tracer not only experiences a translatory motion with mean flow velocity, but an apparent diffusive spreading in the axial direction.

The Taylor approximation to (2.2) is valid if the time necessary for advective effects to appear is large when compared with the time during which radial variations in concentration are reduced via molecular diffusion. Mathematically this equates to the condition

$$\frac{\ell}{v_m} \gg \frac{R^2}{(3.8)^2 D}, \tag{4.1}$$

where the length of pipe the material is spread over is of order ℓ (Taylor, 1953). Taylor heuristically suggested that ratios of 10:1 are permitted in the inequality (4.1) (Taylor, 1954). Taylor's analysis is based on the observation that the transfer of material across planes for which $z_1 = z - \bar{v}t$ is constant, where $\bar{v}$ is the average flow velocity, is dependent only on the radial diffusion of material. Because Taylor's approximation assumes that the radial variation in c is small relative to that in the axial direction, it follows that $\dfrac{\partial c}{\partial z_1}$ is independent of r, and $\dfrac{\partial c}{\partial z_1} \approx \dfrac{\partial Q}{\partial z_1}$ (Taylor, 1954), where Q is the cross-sectional average concentration. It can then be shown that Q, relative to a plane z_1, obeys a diffusive process with effective diffusion coefficient

$$\eta = \frac{\kappa R^2 \bar{v}^2}{D}, \tag{4.2}$$

where κ is Taylor's constant (Aris, 1953), which is 1/48 in Newtonian flow. From the continuity equation for Q, namely

$$\frac{\partial q_c}{\partial z_1} = -\pi R^2 \frac{\partial Q}{\partial t}, \tag{4.3}$$

where q_c denotes the rate of material transfer relative to planes z_1, and ∂_t denotes differentiation with respect to time at a point where z_1 is constant, it follows that the advection-diffusion equation approximation to the concentration dispersion is

$$\frac{\partial Q}{\partial t} + \bar{v}\frac{\partial Q}{\partial z} = \eta \frac{\partial^2 Q}{\partial z^2}. \tag{4.4}$$

This result can also be derived from the more general theory in Aris (1956) for shear dispersion in a pipe of arbitrary cross-section, with an arbitrary velocity profile and spatially varying diffusion coefficient. This more general analysis considers the movement of the centre of gravity of the distribution of solute, and the associated higher moments. This theory indicates that the solute tends to become normally distributed with variance $D + \eta$, i.e., there is an apparent diffusive spreading of the material tracer with effective diffusion coefficient $D + \eta$.

The boundary and initial conditions associated with Taylor's advection-diffusion approximation (4.4) are

$$c(0,t) = c_0(t), \tag{4.5}$$

$$\lim_{z\to\infty} c(z,t) = 0, \tag{4.6}$$

$$c(z,0) = 0. \tag{4.7}$$

Solutions to the Taylor advection-diffusion equation (4.4), along with the boundary and initial conditions (4.5)–(4.7), can be found using Laplace transforms and are of the form

$$Q(z,t) = \int_0^t K(z,t-s)c_0(s)ds, \tag{4.8}$$

where the bounded kernel for this equation is

$$K(z,t) = \frac{z}{2\sqrt{\eta\pi t^3}} \exp\left(\frac{-(z-\bar{v}t)^2}{4\eta t}\right). \tag{4.9}$$

Equation 4.8 defines the operator mapping the concentration c_0 to Q, the average concentration at z.

The Taylor theory allows the partial differential equations (2.2) and (2.7) to be suitably approximated by the advection-diffusion equations

$$\frac{\partial Q_i}{\partial t} + \bar{v}\frac{\partial Q_i}{\partial z} = \eta\frac{\partial^2 Q_i}{\partial z^2},$$
$$z \in [0,\ell_i], \quad t > 0, \quad i \in \{1,4\}. \tag{4.10}$$

Observe that η is significantly larger than the molecular diffusion coefficient D (see Table I). This approximation is valid if (4.1) exhibits a ratio of at least 10:1. However for the geometry and molecules under consideration in the perifusion system, a ratio of at most 3:1 can be obtained. Therefore the Taylor approximation (4.10) is on the borderline of reasonable approximations to (2.2) and (2.7). This approximation is shown in Figure 6.

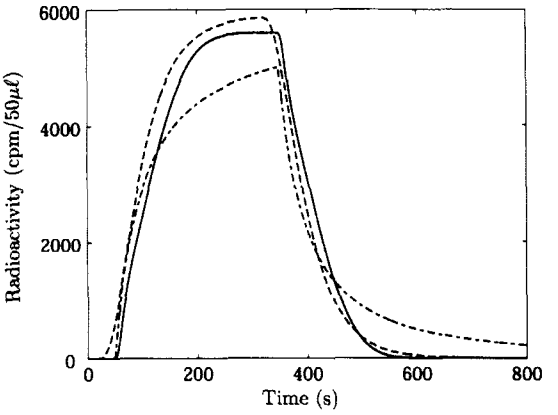

FIGURE 6 Comparison of Q_1 for the full perifusion model (–), the pure shear dispersion model (- – -), and the Taylor approximation (- – -) for a 5 min injection pulse of AVP (c_0)

A notable feature of this diagram is that the concentration peak for the Taylor and full perifusion model is higher than that for the pure dispersion model. This is because the material tracer is able to diffuse from the centre of the pipe into the slower fluid near the pipe boundary, thus counteracting the pure dispersive effect of the velocity gradient. Although the minimum travel time down the pipe is shorter in the Taylor model, the Taylor approximation to the full perifusion model is quite good, given that the approximation is near the suggested borderline of reasonable approximation. We now examine the Taylor advection-diffusion solution sensitivity to the model boundary conditions.

4.2. Boundary conditions

In this section we consider how the model boundary conditions (4.5) and (4.6) affect solutions to the Taylor advection-diffusion equation (4.4). This has previously been investigated by Smith et al. (1991). Our more detailed analysis yields extra insight into the importance of the model boundary conditions, and we discuss this for the perifusion system model.

The boundary condition (4.5) at the pump (see Figure 3) is in fact an approximation to the true boundary condition

$$\bar{v}c_0(t) = \bar{v}c(0,r,t) - D\frac{\partial c}{\partial z}(0,r,t), \qquad (4.11)$$

where c_0 is the concentration time profile of the released hormone at the injection point, and $\bar{v}$ is the average cross-sectional flow velocity. This equation is simply obtained by balancing the concentration flux across the inlet, which includes an advective and a diffusive component. The extra diffusive term in (4.11) was deemed to be particularly important in a model of the perifusion column (Smith et al., 1991). It should be noted that D in (4.11) is the material molecular diffusion coefficient not Taylor's effective diffusion coefficient, η This is because the Taylor theory does not apply to very short lengths of pipe where the flow is yet to develop.

The solution to the Taylor advection-diffusion equation (4.4) with the boundary conditions (4.11) and (4.6) can be found using Laplace transforms, and is expressible in the operator form (4.8), but where now the kernel is

$$K(z,t) = \frac{\bar{v}\sqrt{\eta}}{D}\exp\left(\frac{\bar{v}z}{2\eta} - \frac{\bar{v}^2 t}{4\eta}\right) \left[\frac{1}{\sqrt{\pi t}}\exp\left(\frac{-z^2}{4\eta t}\right) - \varphi\mathrm{erfc}\left(\frac{z}{2\sqrt{\eta t}} + \varphi\sqrt{t}\right)\exp\left(\frac{\varphi z}{\sqrt{\eta}} + \varphi^2 t\right)\right], \qquad (4.12)$$

where erfc is the complementary error function, and

$$\varphi = \frac{(2\eta - D)\bar{v}}{2D\sqrt{\eta}}. \qquad (4.13)$$

Because D is several orders of magnitude smaller than η for the perifusion problem, this change has a very small effect on the model solutions. The Taylor approximations (4.8) to Q_1 for the perifusion system model with kernels (4.9) and (4.12) are shown in Figure 7 (- - -) for a 5 min injection pulse of CRH. The two solutions are indistinguishable. Thus, because advective effects are more significant than diffusive effects at the pipe inlet in the perifusion system, the diffusive term in (4.11) is not important for perifusion system models and can safely be omitted.

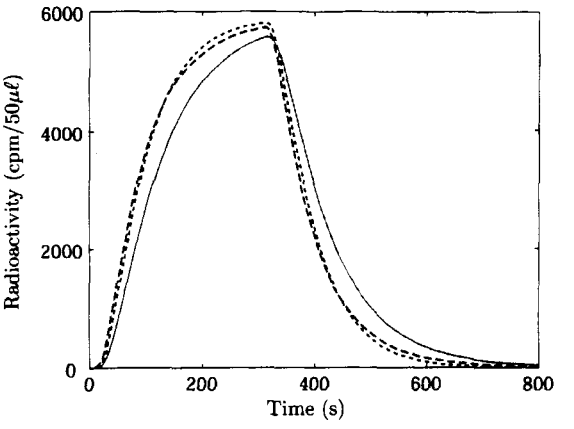

FIGURE 7 Comparison of Q_1 with a 5 minute injection pulse of CRH(C_0) for the Taylor approximations (4.8) with kernels (4.9) (- - -), (4.12) (- - -), (4.14) (···), and the Smith et al. approximation ((4.12) with D = η) (–). The solutions with kernels (4.9) and (4.12) are indistinguishable

However, (4.12) is for a semi-infinite pipe, and for a more realistic finite pipe of length ℓ, the appropriate boundary condition at the pipe exit is Danckwerts' boundary condition (2.9) (i.e., $\frac{\partial c}{\partial z}(\ell,t) = 0$). The solution to this more complicated Taylor advection-diffusion equation, with boundary conditions (4.11) and (2.9), can be found by separation of variables, and can be expressed in the form of (4.8), but where now the kernel is

$$K(z,t) = \sum_{n=-\infty}^{\infty} a_n(-\beta^2 - \lambda_n^2\eta) \exp\left(\beta(z - \frac{\bar{v}t}{2}) - \lambda_n^2\eta t\right)\left[\frac{\alpha\sin\lambda_n z}{\lambda_n} + \cos\lambda_n z\right], \qquad (4.14)$$

where a_n satisfies

$$\int_0^\ell -\exp(-\beta z)\left[\frac{\alpha\sin\lambda_n z}{\lambda_n} + \cos\lambda_n z\right]dz = a_n\int_0^\ell\left[\frac{\alpha\sin\lambda_n z}{\lambda_n} + \cos\lambda_n z\right]^2 dz, \qquad (4.15)$$

and λ_n are solutions to the transcendental equation

$$\lambda^2\tan\lambda\ell - (\alpha+\beta)\lambda - \alpha\beta = 0, \qquad (4.16)$$

with

$$\alpha = \left(\frac{1}{D} - \frac{1}{\eta}\right)\bar{v} \quad \text{and} \quad \beta = \frac{\bar{v}}{2\eta}. \qquad (4.17)$$

The Taylor approximation (4.4) to Q_1 for a 5 min injection pulse of CRH with kernel (4.14) is shown in Figure 7 (···). This solution has a slightly higher peak than the Taylor approximation with kernel (4.12). Thus Danckwerts' boundary condition has a small but distinguishable effect on the perifusion model solution.

The kernels (4.12) and (4.14) simplify significantly if $D = \eta$, and were considered by Smith et al. (1991) as models of the perifusion chamber. The Taylor approximation to Q_1 for a 5 min injection pulse of CRH with kernel (4.12) and $D = \eta$ is shown in Figure 7 (–). This simplifying assumption has a significant effect on the model prediction of Q_1. However this simplifying assumption is not valid, since η is typically at least five orders of magnitude larger than D for the perifusion system problem. Therefore, correct specification of the boundary conditions is particularly important, especially so for the perifusion system.

5. THE INVERSE ADVECTION-DIFFUSION EQUATION

We now consider an inverse problem associated with dispersive flow in pipes. To this end we just consider reconstruction after transmission down the pipe connecting the pump and the perifusion chamber depicted in Figures 1 and 3. The full inverse problem connected with the perifusion apparatus is discussed in Section 6. The inverse problem is that of reconstruction of the source concentration $c_0(t)$ from measurement of $Q_1(t)$, the cross-sectional average concentration at the pipe exit. Under the conditions explained in Section 4.1 (equation 4.1), the dispersive flow of concentration in a pipe can be approximated by the advection-diffusion equation (4.4). Therefore, because analytical solutions to the advection-diffusion problem are available, we consider the source reconstruction problem within this advection-diffusion framework. In this section we also consider the degree of ill-posedness of the associated inverse problem, the problem regularisation, and the construction of numerical schemes for the corresponding stabilised problem.

This inverse advection-diffusion problem has also been analysed by Smith and Wake (1990), and Hào (1996, 1997). Smith and Wake (1990) found an analytical solution to the inverse problem, however this involved an infinite series of time derivatives of the downstream concentration measurement and is of limited practical use. Hào (1996) considered numerical methods based on a mollification method with Dirichlet and de la Vallée Poussin kernels. The solution scheme presented here is based on the method of mollification with a Gaussian kernel. Similar problems excluding advection have been examined extensively (Weber, 1981; Eldén, 1987; Eldén, 1988; Murio and Roth, 1988; Murio, 1989; Guo et al., 1990; Seidman and Eldén, 1990; Murio, 1993; Regińska and Eldén, 1997; Berntsson, 1999).

5.1. Problem conditioning

In this section the inverse problem of reconstruction of the source concentration $c_0(t)$ from $Q_1(t)$, via (4.8) with kernel (4.9), is considered. As we shall see, this inverse problem is always ill-posed for realistic measurement data. This is because measured data can generally only be placed in the space of square integrable functions, L^2, or at most the space of continuous functions, C, and in these function spaces the inverse problem mapping operators are unbounded. It is therefore central to our analysis to show that the inverse problem can be made a well-posed problem. That this can be done is well known, and there are a number of regularisation techniques available. We shall use the method of mollification, based on the treatment of Murio (Murio, 1993).

We now examine the stability of the inverse problem of estimation of c_0, from knowledge of $Q = Q_1(t)$. To understand the degree of ill-posedness it is convenient to perform a Fourier analysis of (4.4). Taking

the Fourier transform of (4.4) with respect to time, we obtain the differential equation

$$i\xi\widehat{Q}(z,\xi) + \bar{v}\widehat{Q}_z(z,\xi) = \eta\widehat{Q}_{zz}(z,\xi), \quad z \in (0,\infty), \quad \xi \in (-\infty,\infty), \tag{5.1}$$

where the Fourier transform of the function Q is defined by

$$\widehat{Q}(\xi) = \frac{1}{\sqrt{2\pi}}\int_{-\infty}^{\infty} Q(t)\exp(-i\xi t)dt. \tag{5.2}$$

By requiring bounded solutions as $z \to \infty$ then implies that the operator mapping $Q \to c_0$ in the Fourier transform domain is

$$\widehat{c_0}(\xi) = \widehat{Q}(\ell,\xi)\exp\left(\frac{-\bar{v}}{2\eta}\ell\right)\exp\left(\sqrt{\frac{|\xi|}{2\eta}}I(\xi,a)\ell\right), \tag{5.3}$$

where

$$I(\xi,a) = (\sqrt{1+a^2}+|a|)^{1/2} + i\sigma(\sqrt{1+a^2}-|a|)^{1/2}, \quad \text{with} \quad a = \frac{\bar{v}^2}{4\xi\eta}, \tag{5.4}$$

for $\sigma = \text{sign}(a)$, and we have used the principal square root. Because $Re(I(\xi,a)) \to 1$ as $|\xi| \to \infty$, it follows from (5.3) that Q is not just a function in $L^2(\mathbb{R})$, but its high frequency behaviour is such that $\|\widehat{Q}\|_2$ decreases at exponential order as $|\xi| \to \infty$. This is because by Parseval's theorem $c_0 \in L^2 \Leftrightarrow \widehat{c_0} \in L^2$. It is readily observed that for a general noise function, $n(t) \in L^2(\mathbb{R})$, assumed to be additive to $Q(t)$ and so perturbating Q, there is no reason to believe that the high-frequency components of $\widehat{n}(\xi)$ will be subject to such rapidly decreasing behaviour, and it therefore follows that there is no guarantee that the resultant $\widehat{c_0}(\xi)$ will be in $L^2(\mathbb{R})$. This illustrates that the inverse signal reconstruction problem is severely ill-posed i.e., $\widehat{Q}$ must decrease faster than any polynomial. It is therefore apparent that Sobolev spaces (Dautray and Lions, 1988) do not suffice in placing quantitative measures on the degree of ill-posedness, so we proceed by defining spaces with exponential weights.

The degree of ill-posedness is apparent if we consider the family of Hilbert spaces E^s furnished with the norm

$$\|u\|_s = \int_{\mathbb{R}} \exp(\sqrt{s|\xi|})|\hat{u}(\xi)|^2 d\xi. \tag{5.5}$$

It then follows that $E^0 = L^2$, $E^{s_1} \subseteq E^{s_2}$ if $s_1 > s_2$, and $E^s = C^\infty$ for $s > 0$. One can also show that if $s_1 > s_2$, then E^{s_1} is dense in E^{s_2}, and E^{s_1} is compactly embedded in E^{s_2} with the compact isometry operator $\mathbb{J}$. The proof is similar to that for Sobolev spaces (Kress, 1989), (p 111). By standard means it follows that if L is a bounded operator then the inverse of the compact operator $(L \circ \mathbb{J})$: $E^0 \to E^0$ is an unbounded operator. Rewriting (5.3) allows the Fourier transform of an operator $\mathbb{T}$ to be defined by

$$\widehat{Q}(\ell,\xi) = \widehat{c_0}(\xi)\exp\left(\frac{\bar{v}\ell}{2\eta}\right)\exp\left(-\sqrt{\frac{\ell^2|\xi|}{2\eta}}I(\xi,a)\right). \tag{5.6}$$

This operator $\mathbb{T}$ is also defined by (4.8). Fourier transform theory than shows that $\mathbb{T}: E^0 \to E^{\ell^2/2\eta}$, and as we deduced previously $(\mathbb{T} \circ \mathbb{J})^{-1}$ is an unbounded operator. From this argument one can therefore deduce that increasing ℓ with η fixed generates a more ill-posed problem. In contrast, increasing η with ℓ fixed generates a more well-posed problem.

We have previously observed that $\|\widehat{Q}\|_2$ decreases at exponential order as $|\xi| \to \infty$. It follows that we can interpret the product of exponential terms in (5.6) as a low-pass filter. A simple measure of the degree of smoothing is the frequency for which the filter attains half-maximum value. For our problem this can be shown to be

$$\xi_{\frac{1}{2}}(\eta,\bar{v}) = \frac{\sqrt{\eta\ln(2)(\ln(2)\eta+\bar{v})}(\bar{v}+2\ln(2)\eta)}{\eta}. \tag{5.7}$$

Because $\xi_{\frac{1}{2}}$ is a strictly increasing function of $\bar{v}$, it follows that the inverse problem is in some sense more well-posed as $\bar{v}$ increases. However for $\bar{v} > 0$, $\lim_{\eta\to\infty}\xi_{\frac{1}{2}} = \lim_{\eta\to 0}\xi_{\frac{1}{2}} = \infty$, and $\xi_{\frac{1}{2}}$ is not a strictly increasing function of η. For fixed $\bar{v}$, $\xi_{\frac{1}{2}}$ is a convex function, and thus attains a minimum

when $\partial_\eta \xi_{\frac{1}{2}} = 0$. The maximum amount of smoothing occurs at this minimum, which is when

$$\eta_{crit} = \frac{(\sqrt{5}-1)}{4\ln(2)}\bar{v}, \tag{5.8}$$

which interestingly contains a golden mean type number. This critical diffusive value separates the inverse problem into two domains, where the diffusive processes respectively increase and decrease the amount of data smoothing respectively. Thus for $\eta \geq \eta_{crit}$ the inverse problem becomes less ill-conditioned as η increases, whereas for $\eta < \eta_{crit}$ the inverse problem becomes more ill-conditioned as η increases. For the perifusion system $\eta_{crit} = 1.5 \times 10^{-3}$ m^2·s^{-1} > η_{CRH}, η_{AVP}, and η_{ACTH} within the pipes, and $\eta_{crit} = 9.5 \times 10^{-5}$ m^2·s^{-1} > D_{CRH}, D_{AVP}, and D_{ACTH} within the chamber (see Table I). Therefore, for the fluid flow rates within the perifusion system, increasing η or D respectively increases the degree of ill-conditioned of the inverse problem associated with the perifusion system.

The advection-diffusion equation approximation to the dispersion in the pipe has generated a considerably more ill-posed inverse problem than the corresponding problem for pure shear dispersive flow discussed in Shorten and Wall (1998). We now investigate the regularisation of this more ill-posed inverse problem.

5.2. Problem regularisation

The problem is to get a regularised approximation to the function c_0 when given a modified function Q_m; where due to measurement difficulties the true function Q, has been corrupted by a noise function n, so that

$$Q_m(t) = Q(t) + n(t), \quad t \in I.$$

The functions Q, and n, are defined on the interval I= [0, T], for a given value of $T > 0$. To proceed, we extend the data Q_m to the interval I_δ = [-3δ, 3δ + T], and define the mollifier of Q, $J_\delta Q$, with mollification radius δ by

$$J_\delta f(x) = (\rho_\delta * f)(x) = \int_{-\infty}^{\infty} \rho_\delta(x-s)f(s)ds,$$
$$\cong \int_{x-3\delta}^{x+3\delta} \rho_\delta(x-s)f(s)ds,$$
$$\text{with} \quad \rho_\delta(x) = \frac{1}{\delta\sqrt{\pi}} e^{-x^2/\delta^2}, x \in \mathbb{R}. \tag{5.9}$$

The following elementary result is central to our stability proof (Murio, 1993).

Lemma: *Murio's Consistency. With $f \in C^1$ and if $\|f'\|_2 \leq M$ then*

$$\|(J_\delta f) - f\|_2 \leq \frac{\delta M}{2}. \tag{5.10}$$

This consistency result shows that as $\delta \to 0$, then $(J_\delta f) \to f$.

To convert this problem into a well-posed problem consider the effect of mollification of the measured function Q, that is look at the solution to the problem when Q is replaced by $J_\delta Q$. Due to the linearity of the direct problem, c_0 is then replaced by $J_\delta c_0$, and it can be shown that (5.3) becomes

$$\widehat{J_\delta c_0}(\xi) = \frac{1}{\sqrt{2\pi}} \exp\left(\frac{-\bar{v}}{2\eta}\ell\right) \exp\left(\sqrt{\frac{|\xi|}{2\eta}} I(\xi,a)\ell - \frac{\xi^2\delta^2}{4}\right) \widehat{Q}(\xi). \tag{5.11}$$

It is now seen that the effect of the mollification is to bound the growth of the exponential function for large values of $|\xi|$. In fact

$$\left|\exp\left(\frac{-\bar{v}}{2\eta}\ell\right) \exp\left(\sqrt{\frac{|\xi|}{2\eta}} I(\xi,a)\ell - \frac{\xi^2\delta^2}{4}\right)\right| <$$
$$\exp(f(\delta)) = \exp\left(\frac{\bar{v}}{2} + \frac{3}{4\eta^{\frac{2}{3}}\delta^{\frac{2}{3}}}\right), \tag{5.12}$$

with $f > 0$ and bounded above for non-zero η and δ. Related inverse problems when $\eta = 0$ are examined in Wall and Lundstedt (1998). It follows that

$$\|(\widehat{J_\delta c_0}) - (\widehat{J_\delta \bar{c_0}})\|_2^2 \leq \frac{\exp(f(\delta))}{\sqrt{2\pi}} \|\widehat{Q}_m - \widehat{Q}\|_2^2, \tag{5.13}$$

where $\overline{c_0}$ corresponds to c_0 when Q is replaced by Q_m. The stability result then follows directly from Parseval's theorem.

Lemma 5.1 *If* Q, $Q_m \in L^2$ *then*

$$\|(J_\delta c_0)-(J_\delta \overline{c_0}\|_2^2 \leq \frac{\exp(f(\delta))}{\sqrt{2\pi}}\|Q_m-Q\|_2^2. \quad (5.14)$$

We see the mollification method provides the inverse mapping operator with a Lipschitz continuity result, when the data $Q_\mathrm{m} \in C$, provided $\delta > 0$ is fixed. Furthermore as $\|Q_\mathrm{m}\text{-}Q\| \to 0$, the parameter δ can be reduced, and the consistency error is then decreased, provided $Q \in C^1$. Lemma 5.1 and Murio's consistency lemma then provides the well-posedness of the inverse problem:

Theorem 5.2. *The mollified inverse problem is stable with respect to perturbations in the data* Q. *If the exact boundary function* $Q \in C^1$ *with* $\|Q'\|_2 < M$ *then the solution* $J_\delta \overline{c_0}$ *to the mollified inverse problem satisfies*

$$\|(J_\delta \overline{c_0}) - c_0\|_2^2 \leq \frac{\exp(f(\delta))}{\sqrt{2\pi}}\|Q_m - Q\|_2^2 + \frac{\delta M}{2}. \quad (5.15)$$

Having shown that the mollification procedure provides a well-posed formulation of the inverse problem, we now consider a numerical scheme to compute the regularised solution.

5.3. Numerical methods

We now investigate stable marching schemes to solve the regularised inverse problem. The stabilised problem under consideration is to find $J_\delta c_0(0,t) = J_\delta Q(0, t)$ for times t of interest, and some $\delta > 0$, given that $J_\delta Q(z, t)$ satisfies

$$\begin{aligned} \frac{\partial(J_\delta Q)}{\partial t} + \bar{v}\frac{\partial(J_\delta Q)}{\partial z} &= \eta\frac{\partial^2(J_\delta Q)}{\partial z^2}, \quad t > 0, \\ (J_\delta Q)(z,0) &= 0, \quad z > 0, \\ (J_\delta Q)(\ell,t) &= J_\delta Q_m(t), \quad t \geq 0, \end{aligned} \quad (5.16)$$

where Q_m is the noise corrupted data measurement. We now consider approximate solutions to (5.16) by means of finite difference equations. Consider the uniform discretisation of the z-t plane: $\{(z_n = nh, t_j = jm), n = 0,1, \ldots, N; Nh = \ell\, j = 0,1, \ldots, M; Mm = L > \ell\}$, where L depends on h and m in a way to be specified later. If we define the grid function $V_j^n = J_\delta Q(z_n, t_j)$, then the partial differential equation in (5.16) can be approximated by the consistent finite-difference scheme

$$\begin{aligned} &\frac{1}{2m}(V_{j+1}^n - V_{j-1}^n) + \frac{\bar{v}}{h}(V_j^n - V_j^{n-1}) = \\ &\frac{\eta}{h^2}(V_j^{n+1} - 2V_j^n + V_j^{n-1}), \end{aligned} \quad (5.17)$$

for $j = 1,2, \ldots, M$, $n = 1,2, \ldots, N$, where $V_j^N = J_\delta Q_m(t_j)$, $j = 0,1, \ldots, M$ and $V_0^n = 0$, $n = 0,1, \ldots, N$. This space marching scheme has local truncation error $\mathcal{O}(h + m^2)$ as $h, m \to 0$, and requires two initial conditions, V_j^N and V_j^{N+1}. The second data function, $J_\delta G_m = J_\delta Q(\ell + h, t)$, can easily be obtained by solving the well-posed direct problem (4.8) in the quarter plane $z > \ell$, $t > 0$, with initial condition $Q(x, 0) = 0$, and boundary condition $Q(\ell, t) = J_\delta Q_m$. Note that as we march back in space, at each step we must drop the estimation of the concentration profile by one temporal discretisation step. To determine the solution V_j^0 on the interval $[0, T]$ therefore requires that $L = T + \ell m/h$. For h sufficiently small, the space marching scheme in (5.17) can be shown to be consistent with the stabilised problem (5.16) and stable (see Appendix A).

6. PULSE RECONSTRUCTION IN PERIFUSION EXPERIMENTS

We now consider the inverse problem of predicting the input concentration c_0 from knowledge of the output concentration measurement Q_4. This inverse problem can be divided into four smaller inverse problems; three inverse advection-diffusion equations and one inverse mixing problem. The deconvolution procedure for the inverse advection-diffusion equation has been discussed in Sections 5. The results in this section were obtained with a mollification radius of $\delta = 62.5$ s, and mesh intervals of $N = 50$, and $M = 250$ respectively (see Section 5).

The full inverse problem discussed here requires the solution to an inverse mixing problem, which we now briefly discuss. This interesting, and useful inverse problem is the reconstruction of Q_1 from measurement of Q_2. In general this is severely ill-posed. However in the radial-independent case with $Q_1(r, t) = Q_1(t)$, or equivalently $v(r) = \bar{v}$, (2.3) simplifies significantly. From (2.3) it then follows that the ill-posedness in computing $Q_1(t)$ from $Q_2(t)$ is *equivalent* to a differentiation. A simple procedure for numerically computing Q_1 is to compute the derivative in (2.3) in a stable manner using the mollification method (Murio, 1989), which is outlined in Section 5.2.

The full deconvolution process is shown in Figure 8, where a 2 min experimental curve from Figure 4 D is used as the concentration measurement Q_4. The predicted concentration at the cells, chamber entrance, and pump are shown in Figure 8 B, C, and D respectively. The input pulse is unable to be completely reconstructed for two reasons. Firstly the model is an approximation to the actual system, and we have used the Taylor approximation to this model. The second and more important reason is that because the inverse problem is ill-posed, we cannot expect to reconstruct the high frequency components of the input concentration. What we have reconstructed is a reasonable approximation to the mollified input.

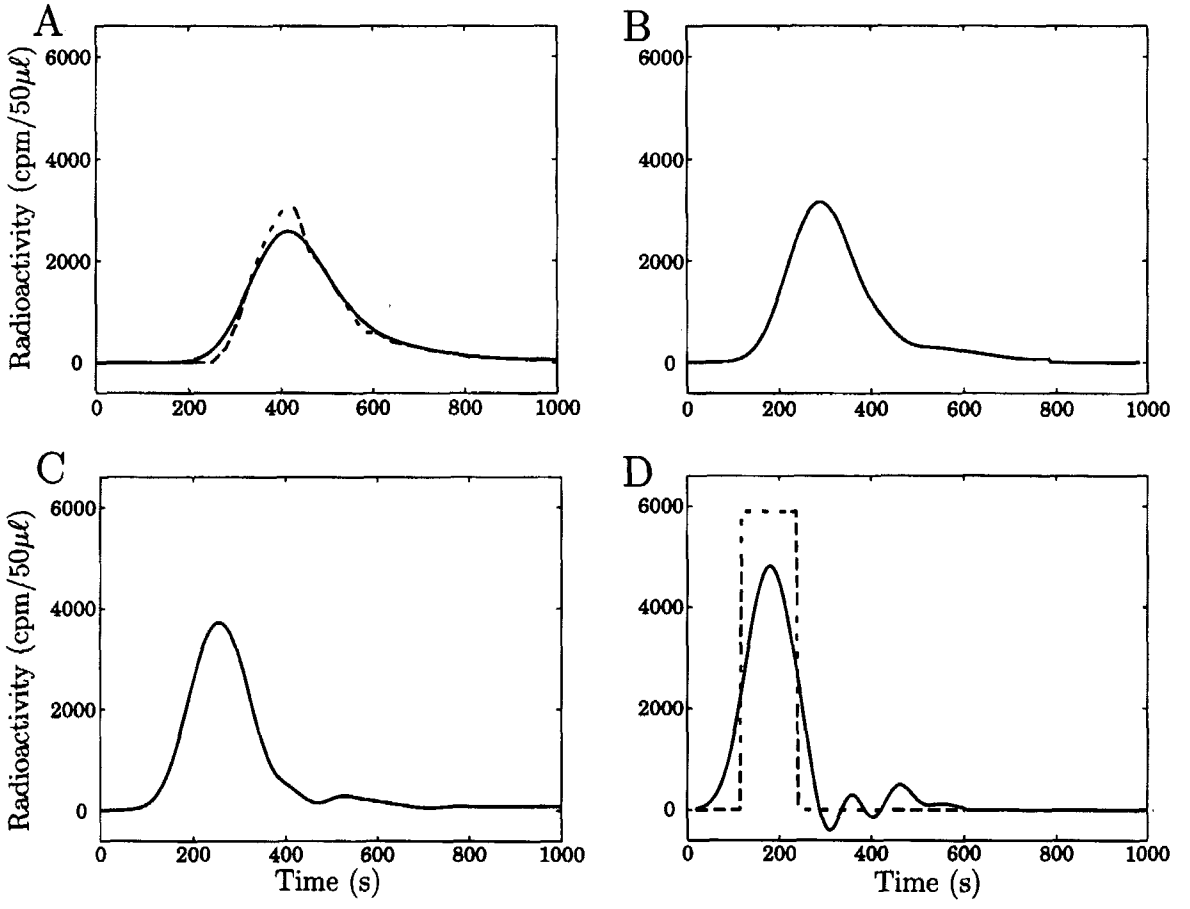

FIGURE 8 Prediction of the input concentration from an output concentration measurement in a 2 min pulse validation experiment. (A) The output concentration measurement Q_4 (- – -), and its mollification (-). (B) The predicted concentration at the cells (Q_2). (C) The predicted chamber entrance concentration (Q_1). (D) The predicted input concentration (c_0) (–), and the actual input concentration (- – -)

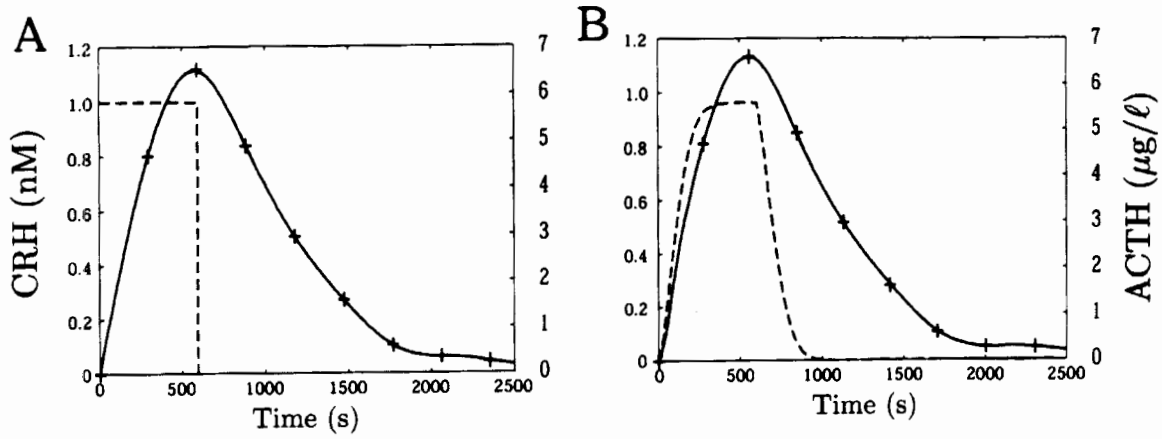

FIGURE 9 CRH-induced ACTH secretion data. (A) The 10 min CRH input pulse (c_0) of 0.1 nM (- – -), and the ACTH measurement (Q_4) collected in 5 min fractions (+), along with a cubic spline fit (–). (B) Predicted CRH concentration profile at the pituitary cells (Q_2) (- – -), and the predicted ACTH concentration profile secreted by the pituitary cells (-)

The reconstructions for the 1 and 5 min pulses in Figures 5 B, D are similar (not shown).

7. CRH-INDUCED ACTH DATA ENHANCEMENT

We have observed that there is a certain amount of dispersion in the signal travelling down the perifusion system, particularly for pulses of short duration. The methods developed in Sections 3 and 6 are now used to account for this in CRH-induced ACTH measurements from equine corticotrophs (Evans et al., 1993), (p 396).

In these experiments a 10 min CRH input pulse of 0.1 nM is input into the perifusion system (Figure 9 A (- - -)). Using the direct problem solutions from (2.2) and (2.4), we can then predict the CRH concentration profile that the cells are exposed to (see Figure 9 B (- - -)). Secondly, given the collected ACTH concentration profile measurement, the ACTH concentration profile secreted by the pituitary cells can be estimated using the theory developed in Section 5. The ACTH measurement collected in 5 min fractions is shown in Figure 9 A (+), along with a cubic spline fit (–), and the reconstruction is shown in Figure 9 B(–). Because the secreted ACTH concentration profile in Figure 9 B is of long duration, the dispersion in the ACTH concentration profile is minimal.

The deconvolution in Figure 9 B supports the concentration dependent, rapid activation of CRH-induced ACTH secretion, and a delayed return to basal ACTH secretion following the termination of the CRH pulse. This contrasts with the raw data in Figure 9 A, which suggests a significant delay in activation of the CRH-induced ACTH secretion. Our deconvolution interpretation agrees with data from the microperifusion system, which allows the delivery of square wave pulses of CRH to the cells, ACTH measurements very near the cells, and a much shorter sampling interval of 5 s (Watanabe and Orth, 1987). The ACTH responses for 3 min CRH pulses from the microperifusion system are shown in Figure 10. The onset of ACTH secretion is rapid compared with the delay in the return to basal ACTH secretion levels following the termination in the CRH pulse.

The decay in ACTH secretion following the termination of the CRH pulse can be suitably approximated by an exponentially decaying function. The rate of decay in this function is then a simple measure of the time for ACTH secretion to return to basal levels. This rate of decay can be more accurately determined

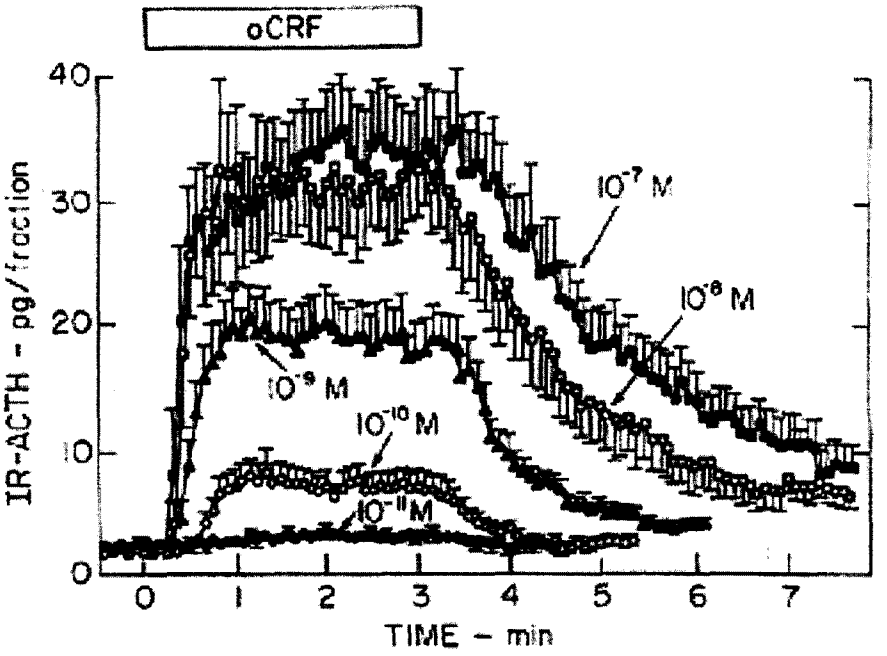

FIGURE 10 Experimental ACTH output collected in 5 s fractions from ovine pituitary corticotroph cells for a 3 min CRH pulse (indicated by the horizontal oCRF bar). Higher concentrations of CRH induce a greater ACTH response. The onset of ACTH secretion is rapid compared to the delay in ACTH secretion returning to basal following the termination in the CRH pulse. Data from Watanabe and Orth (1987), p1139 (reproduced by permission of the Society for Endocrinology)

from the deconvolved data, particularly for data obtained from short CRH pulses. Interestingly this rate of decay appears to depend on [CRH] (see Figure 10).

For the raw data in Figure 9, one can associate 1 nM CRH with an ACTH secretion rate of about 6.5 mg/ℓ. Because the cells are nearly exposed to 1 nM CRH, there is little error in this statement. However, due to dispersion, similar associations between the injected CRH concentration and the measured ACTH concentration for shorter CRH pulses will not be valid (see Figure 5 for a graphical interpretation of this). This can be partially alleviated using the deconvolution procedure developed in this paper.

The cell does not see a square wave CRH profile, and it is difficult to predict what the cell would secrete given a square wave CRH profile. To do so would require knowledge of the cellular functional relationship between CRH and ACTH secretion. However this relationship is not known, and in fact the experiments are designed to infer this relationship. One can argue that cells *in vivo* are never exposed to square wave hormone pulses. This is because the hormone must travel in the bloodstream, and therefore a certain amount of signal dispersion must occur. However the microperifusion system is superior to the perifusion system, as it enables the delivery of a wider range of CRH inputs, with higher resolution in the ACTH secretion rate. Justifiably this superior system is more expensive to setup. However, because the cellular system is nonlinear, knowledge of the square wave response does not provide knowledge of the ACTH output for arbitrary CRH input concentrations.

8. DISCUSSION

The major drawback of the perifusion system derives from the dispersion and mixing of the material tracer within the pipe. This is particularly significant for input pulses of short duration. We have constructed a mathematical model of the fluid flow in the perifusion system, and observed that it explains a number of observable features in the measured concentration profile. We have also constructed a useful approximation to the model, the advection-diffusion equation, and outlined under what conditions the approximation is valid and how the associated parameters relate to measurable quantities.

The major drawbacks of the perifusion system have been highlighted, and a number of improvements can be based on these drawbacks. In order to circumvent the dispersion in the perifusion system a number of improved systems have been devised, notably the microperifusion apparatus designed by Watanabe and Orth (1987), which eliminates the pipes altogether. One can also decrease the dispersion in the pipes by using a pseudoplastic fluid, or by increasing the fluid flow rate. However the pituitary cells do not behave normally if the fluid flow rate is too large, so this is not a viable option. Decreasing the cell chamber volume will also reduce the amount of dispersion in the input concentration profile.

We have also introduced a class of inverse problems in order to deconvolve, or take account of the introduced experimental errors in the perifusion apparatus. These ill-posed inverse problems involve the estimation of a temporally varying upstream concentration from measurement of a cross sectional average material concentration at some downstream location. Due to the ill-posedness of this inverse problem, there is a limit to the degree of data improvement. However, in contrast with the raw data, this deconvolution supports the concentration dependent, rapid activation of CRH-induced ACTH secretion, along with a delayed return to basal ACTH secretion following the termination of the CRH pulse. This interpretation agrees with data obtained from the microperifusion system.

Acknowledgements

This work was supported by a Marsden grant administered by the Royal Society of New Zealand, and (PRS) acknowledges the receipt of a University of Canterbury doctoral scholarship. We thank M.J. Evans and D.R. Mason for helpful discussions and data from their perifusion systems. We also thank H-Q Bui for discussions on Sobolev spaces.

References

Alexander S.L., Irvine C.H.G., Liversey J.H. and Donald R.A. (1988). The effect of isolation stress on the concentrations of arginine vasopressin, α-melanocyte-stimulating hormone and ACTH in the pituitary venous effluent of the normal horse. *Journal of Endocrinology*, 116, 325–334.

Aris R. (1953). On the dispersion of a solute in a fluid flowing through a tube. *Proceedings of the Royal Society of London: Series A, Mathematical and Physical Sciences*, 235, 67–77.

Berntsson F. (1999). A spectral method for solving the sideways heat equation. *Inverse Problems*, 15, 891–906.

Dautray R. and Lions J.L. (1988). *Mathematical Analysis and Numerical Methods for Science and Technology*, volume 2. Springer-Verlag.

Eldén L. (1987). Approximations for a Cauchy problem for the heat equation. *Inverse Problems*, 3, 263–273.

Eldén L. (1988). Hyperbolic approximations for a Cauchy problem for the heat equation. *Inverse Problems*, 4, 59–70.

Evans M.J. (2000). Personal communication.

Evans M.J., Brett J.T., McIntosh R.P., McIntosh J.E.A., McLay J.L., Livesey J.H. and Donald R.A. (1988). Characteristics of the ACTH response to repeated pulses of corticotropin-releasing factor and arginine vasopressin *in vitro*. *Journal of Endocrinology*, 117, 387–395.

Evans M.J., Brett J.T., McIntosh R.P., McIntosh J.E.A., Roud H.K., Livesey J.H. and Donald R.A. (1985). The effect of various corticotropin-releasing factor trains on the release of adrenocorticotropin, β-endorphin, and β-lipoprotein from perfused pituitary ovine pituitary cells. *Endocrinology*, 117, 893–899.

Evans M.J., Marshall A.G., Kitson N.E., Summers K., Liversey J.H. and Donald R.A. (1993). Factors affecting ACTH release from perifused equine anterior pituitary cells. *Journal of Endocrinology*, 137, 391–401.

Guo L., Murio D.A. and Roth C. (1990). A mollified space marching finite differences algorithm for the inverse heat conduction problem with slab symmetry. *Computers & Mathematics with Applications*, 19(7), 75–89.

Hào D.N. (1996). A mollification method for a noncharacteristic Cauchy problem for a parabolic equation. *Journal of Mathematical Analysis and Applications*, 199, 873–909.

Hào D.N. and Reinhardt H.J. (1997). On a sideways parabolic equation. *Inverse Problems*, 13, 297–309.

Kao R.R. (1989). *Mathematical models of perifusion column experiments*. Master's thesis, University of Guelph, Ontario, Canada.

Knudsen J.G. and Katz D.L. (1958). *Fluid Dynamics and Heat Transfer*. McGraw-Hill, New York.

Kress R. (1989). *Linear Integral Equations*. Springer-Verlag, Berlin.

LeBeau A.P., Robson A.B., McKinnon A.E., Donald R.A. and Sneyd J. (1997). Generation of action potentials in a mathe-

matical model of corticotrophs. *Biophysical Journal*, 73(3), 1263–1275.

Li Y., Stojilković S., Keizer J. and Rinzel J. (1997). Sensing and refilling calcium stores in an excitable cell. *Biophysical Journal*, 72, 1080–1091.

Linz P. (1985). *Analytical and Numerical Methods for Volterra Equations*. SIAM, Philadelphia.

Mason D.R. (2000). Personal communication.

McIntosh J.E.A. and McIntosh R.P. (1983). Influence of the characteristics of pulses of gonadotrophin releasing hormone on the dynamics of luteinizing hormone release from perifused sheep pituitary cells. *Journal of Endocrinology*, 98, 411–421.

McIntosh J.E.A., McIntosh R.P. and Kean R.J. (1984). Microcomputer-controlled device for delivering hormone stimulation to cell suspensions in perifusion: release of luteinising hormone from sheep pituitary cells. *Medical & Biological Engineering & Computing*, pp. 259–262.

Murio D.A. (1989). The mollification method and the numerical solution of the inverse heat conduction problem by finite differences. *Computers & Mathematics with Applications*, 17(10), 1385–1396.

Murio D.A. (1993). *The Mollification Method and the Numerical Solution of Ill-Posed Problems*. John Wiley & Sons, Inc, New York.

Murio D.A. and Roth C. (1988). An integral solution for the inverse heat conduction problem after the method of Weber. *Computers & Mathematics with Applications*, 15, 39–51.

Phillips C.G. and Kaye S.R. (1996). A uniformly asymptotic approximation for the development of shear dispersion. *Journal of Fluid Mechanics*, 329, 413–443.

Regińska T. and Eldén L. (1997). Solving the sideways heat equation by a wavelet-Galerkin method. *Inverse Problems*, 13, 1093–1106.

Seidman T.I. and Eldén L. (1990). An "optimal filtering" method for the sideways heat equation. *Inverse Problems*, 6, 681–696.

Shorten P.R. (2000). *Mathematical models of pituitary corticotrophs and perifusion experiments*. Ph. D. thesis, University of Canterbury, Christchurch, New Zealand.

Shorten P.R., Robson A.B., McKinnon A.E. and Wall D.J.N. (2000). CRH-induced electrical activity and calcium signaling in pituitary corticotrophs. *Journal Theoretical Biology*, 206(3): 395–405.

Shorten P.R. and Wall D.J.N. (1998). Signal restoration for a mass transport problem involving shear dispersion. *Inverse Problems*, 14, 1021–1032.

Shorten P.R. and Wall D.J.N. (2000). Fluid velocity profile reconstruction for non-Newtonian shear dispersive flow. *Journal of Applied Mathematics & Decision Sciences*, in Press.

Smith R. (1988). Entry and exit conditions for flow reactors. *IMA Journal of Applied Mathematics*, 41, 1–20.

Smith W.R. and Wake G.C. (1990). Mathematical analysis: An inverse problem arising in convective-diffusive flow. *IMA Journal of Applied Mathematics*, 45, 225–231.

Smith W.R., Wake G.C., McIntosh J.E.A., McIntosh R.P., Pettigrew M. and Kao R. (1991). Mathematical model of perifusion data: models predicting elution concentration. *American Journal of Physiology – Regulatory, Integrative and Comparative Physiology*, 261(1), R247-R256.

Strikwerda J.C. (1989). *Finite difference schemes and partial differential equations*. Wadsworth, Inc., California.

Taylor G.I. (1953). Dispersion of soluble matter in solvent flowing slowly through a tube. *Proceedings of the Royal Society of London: Series A, Mathematical and Physical Sciences*, 219, 186–203.

Taylor G.I. (1954). Conditions under which dispersion of a solute in a stream of a solvent can be used to measure molecular diffusion. *Proceedings of the Royal Society of London: Series A, Mathematical and Physical Sciences*, 225, 473–477.

Veldhuis J.D. (1991). Temporal architecture of in vivo endocrine glandular signaling: obtaining a secretory blueprint by deconvolution analysis. *Molecular and Cellular Endocrinology*, 77, C63-C71.

Wall D.J.N. and Lundstedt J. (1998). Inverse source problems involving the one-way wave equation: Source function reconstruction. *Wave Motion*, 27, 55–77.

Washburn E.W. (1926). *International Critical Tables of Numerical Data, Physics, Chemistry and Technology*. volume 5, pp. 63–70. McGraw-Hill, New York.

Watanabe T. and Orth D.N. (1987). Detailed kinetic analysis of adrenocorticotropin secretion by dispersed rat anterior pituitary cells in a microperifusion system: Effects of ovine corticotropin-releasing factor and arginine vasopressin. *Endocrinology*, 121(3), 1133–1145.

Watt S.D. and Roberts A.J. (1995). The accurate dynamic modeling of contaminant dispersion in channels. *SIAM Journal of Applied Mathematics*, 554, 1016–1038.

Weast R.C. (1999). *CRC handbook of chemistry and physics*. CRC Press, Cleveland, Ohio, 80th edition.

Weber C.F. (1981). Analysis and solution of the ill-posed inverse heat conduction problem. *International Journal of Heat and Mass Transfer*, 24, 1783–1792.

APPENDIX A. INVERSE PROBLEM REGULARISATION

Theorem A.1. *For h sufficiently small, the space marching scheme in (5.17), with initial conditions $V^N(t) = J_\delta Q_m(t)$ and*

$$V^{N+1}(t) = \int_0^t K(h, t-s) J_\delta Q_m(s) ds, \quad \text{(A.1)}$$

where K is given by (4.9), is consistent with the stabilised problem (5.16), and is stable.

Proof In order to analyse the stability of the marching scheme (5.17), we consider the following equivalent scheme:

$$\frac{1}{h}(V_j^n - V_j^{n-1}) = U_j^{n-1} \quad \text{(A.2)}$$

$$\frac{1}{2m}(V_{j+1}^n - V_{j-1}^n) + \bar{v} U_j^{n-1} = \frac{\eta}{h}(U_j^n - U_j^{n-1}),$$

where U can be interpreted as an intermediate flux variable. The discrete Fourier transform, $\tilde{f}$, of $f_j = f(jm)$, for j an integer, is defined by

$$\tilde{f} = \sum_i f_j \exp(ijmw), \quad 0 \le |w| \le \pi/m. \quad \text{(A.3)}$$

Taking the discrete Fourier transform of (A.2) we have

$$\begin{bmatrix} \tilde{U}^{n-1} \\ \tilde{V}^{n-1} \end{bmatrix} = \begin{bmatrix} \dfrac{\eta}{\bar{v}h + \eta} & \dfrac{-ih\sin(wm)}{m(\bar{v}h+\eta)} \\ \dfrac{-\eta h}{\bar{v}h+\eta} & 1 - \dfrac{ih^2 \sin(wm)}{m(\bar{v}h+\eta)} \end{bmatrix} \begin{bmatrix} \tilde{U}^n \\ \tilde{V}^n \end{bmatrix},$$

where for h sufficiently small

$$\max(|\tilde{V}^{n-1}|, |\tilde{U}^{n-1}|) \le \left(1 + h + \frac{h|w|}{\eta}\right) \max(|\tilde{V}^n|, |\tilde{U}^n|), \quad \text{(A.4)}$$

where $|\sin(wm)| \le m|w|$. The following stability argument is based on a similar argument in Murio, 1993 (p 80). It follows that

$$\max(|\tilde{V}^0|, |\tilde{U}^0|) \le \left(1 + h + \frac{h|w|}{\eta}\right)^N \max(|\tilde{\rho}_\delta \tilde{Q}_m|, |\tilde{\rho}_\delta \tilde{F}_m|), \quad \text{(A.5)}$$

where F_m is the flux at $z = \ell$, which can be estimated through the second kind operator

$$F_m(t) = \frac{1}{h_1}\left(\int_0^t K(h_1, t-s) Q_m(s) ds - Q_m(t)\right), \quad t \in [0, L], \quad \text{(A.6)}$$

where K is given by (4.9), and $h_1 > 0$ is fixed. It follows from standard theory that $\|F_m\|_2$ is bounded by $c_1 \|Q_m\|_2$, for some fixed positive constant c_1 (Linz, 1985), (p 40). Therefore

$$|\tilde{V}^0|^2, |\tilde{U}^0|^2 \le \left(1 + h + \frac{h|w|}{\eta}\right)^{2N} |\tilde{\rho}_\delta| \, (|\tilde{Q}_m|^2 + |\tilde{F}_m|^2). \quad \text{(A.7)}$$

From Poisson's summation formula

$$\tilde{\rho}_\delta(w) = \sum_{j=-\infty}^{\infty} \hat{\rho}_\delta\left(w + \frac{2\pi j}{m}\right), \quad 0 \le |w| \le \frac{\pi}{m}, \quad \text{(A.8)}$$

we can show that

$$|\tilde{\rho}_\delta(w)| \le 4 \exp\left(\frac{-w^2\delta^2}{4}\right), \quad \text{(A.9)}$$

for $\delta \ge m$. Therefore integrating (A.7) with respect to w, and taking square roots we have

$$\max(\|\tilde{V}^0\|_2, \|\tilde{U}^0\|_2) \le 4 \sup_{0 \le |w| \le \frac{\pi}{m}} \left[\exp\left(\ell + \frac{\ell|w|}{\eta} - \frac{w^2\delta^2}{4}\right)\right] (\|\tilde{Q}_m\|_2 + \|\tilde{F}_m\|_2), \quad \text{(A.10)}$$

where $Nh = \ell$, and $(1 + x)^N < \exp(Nx)$. It follows that if $\delta \ge \sqrt{2m/\pi}$ then

$$\max(\|\tilde{V}^0\|_2, \|\tilde{U}^0\|_2) \le 4 \exp\left(\ell + \frac{\ell^2}{\eta^2\delta^2}\right) (\|\tilde{Q}_m\|_2 + \|\tilde{F}_m\|_2), \quad \text{(A.11)}$$

and the stability result for fixed $\delta > 0$ follows from Parseval's equality. □